Citation for published version:
Mameli, A, Parish, J, Dogan, T, Gelinik, G, Snook, M, Straiton, A, Johnson, AL & Kronemeijer, AJ 2022, 'High-Throughput Atomic Layer Deposition of p-Type SnO Thin Film Transistors Using Tin(II)bis(tert-amyloxide)', *Advanced Materials Interfaces*, vol. 9, no. 9, 2101278. https://doi.org/10.1002/admi.202101278

DOI:
10.1002/admi.202101278

Publication date:
2022

Document Version
Peer reviewed version

Link to publication

This is the peer reviewed version of the following article: Mameli, A., Parish, J. D., Dogan, T., Gelinck, G., Snook, M. W., Straiton, A. J., Johnson, A. L., Kronemeijer, A. J., High-Throughput Atomic Layer Deposition of P-Type SnO Thin Film Transistors Using Tin(II)bis(tert-amyloxide). Adv. Mater. Interfaces 2022, 2101278., which has been published in final form at https://doi.org/10.1002/admi.202101278. This article may be used for non-commercial purposes in accordance with Wiley Terms and Conditions for Use of Self-Archived Versions. This article may not be enhanced, enriched or otherwise transformed into a derivative work, without express permission from Wiley or by statutory rights under applicable legislation.

University of Bath

Alternative formats

If you require this document in an alternative format, please contact:
openaccess@bath.ac.uk

General rights
Copyright and moral rights for the publications made accessible in the public portal are retained by the authors and/or other copyright owners and it is a condition of accessing publications that users recognise and abide by the legal requirements associated with these rights.

Take down policy
If you believe that this document breaches copyright please contact us providing details, and we will remove access to the work immediately and investigate your claim.

Download date: 03. Mar. 2023

High-Throughput Atomic Layer Deposition of p-Type SnO Thin Film Transistors Using Tin(II)bis(tert-amyloxide)

Alfredo Mameli, James D. Parish, Tamer Dogan, Gerwin Gelinck, Michael W. Snook, Andrew J. Straiton, Andrew L. Johnson,** and Auke J. Kronemeijer*

Dr. A. M. Author 1
TNO / Holst Centre, High Tech Campus 31, 5656 AE, Eindhoven, The Netherlands
E-mail: alfredo.mameli@tno.nl

Dr. J.D.P. Author 2
Department of Chemistry, University of Bath, Claverton Down, Bath BA2 7AY, U.K.

Dr. T.D. Author 3
Applied Physics, Eindhoven University of Technology, 5600 MB Eindhoven, The Netherlands

Prof. G.G. Author 4
TNO / Holst Centre, High Tech Campus 31, 5656 AE, Eindhoven, The Netherlands
Applied Physics, Eindhoven University of Technology, 5600 MB Eindhoven, The Netherlands

M.W.S. Author 5
Department of Chemistry, University of Bath, Claverton Down, Bath BA2 7AY, U.K.

A.J.S. Author 6
Department of Chemistry, University of Bath, Claverton Down, Bath BA2 7AY, U.K.

Prof. A.L.J. Author 7
Department of Chemistry, University of Bath, Claverton Down, Bath BA2 7AY, U.K.
E-mail: chsalj@bath.ac.uk

Dr. A.J.K. Author 8
TNO / Holst Centre, High Tech Campus 31, 5656 AE, Eindhoven, The Netherlands

Keywords: p-type transistor, tin monoxide (SnO), spatial atomic layer deposition, precursor, tin(II) alkoxide

Spatial atomic layer deposition (sALD) of p-type SnO has been demonstrated using a novel liquid ALD precursor, tin(II)-bis(tert-amyloxide), $Sn(TAA)_2$, and H_2O as the co-reactant in a process which shows an increased deposition rate when compared to conventional temporal ALD. Compared to previously reported temporal ALD chemistries for the deposition of SnO,

deposition rates of up to 19.5 times higher were obtained using $Sn(TAA)_2$ as a precursor in combination with atmospheric pressure sALD. Growths per cycle of 0.55 Å and 0.09 Å were measured at deposition temperatures of 100 °C and 210 °C, respectively. Common-gate thin film transistors (TFTs), fabricated using sALD with $Sn(TAA)_2$ resulted in linear mobilities of up to 0.4 $cm^2V^{-1}s^{-1}$ and on-/off-current ratios, $I_{On}/I_{Off} > 10^2$. The combination of enhanced precursor chemistry and improved deposition hardware enabled unprecedently high deposition rate ALD of p-type SnO, representing a significant step towards high-throughput p-type TFT fabrication on large area and flexible substrates.

1. Introduction

Transparent semiconducting metal-oxides have become the foundation of devices such as thin-film transistors (TFTs), solar cells, photodetectors and memories.[1–4] The majority of these devices rely on n-type semiconducting compounds (*e.g.* InGaZnO, InZnO, ZnSnO, ZnO), for which materials and processes are well established. In contrast, the development of reliable and high performance p-type oxide materials has proven itself to be challenging owing to their inherently high density of interfacial defect states and comparably poor electrical performance,[5] which in turn hampers the effective combination of p- and n-type oxides within complementary metal oxide semiconductor (CMOS). [6–8] Material/interface engineering, in addition to effective doping strategies involving scalable and highly precise processing technology on large areas, have been deemed necessary to advance the development of p-type oxide materials.[5]

Atomic layer deposition (ALD) is a layer-by-layer thin film deposition method that allows for atomic-level control over thickness and material/interface properties, resulting in conformal and uniform deposition over large areas, and high aspect ratio substrates.[9,10] Such

unique features stem from the fact that ALD relies on cyclic and self-limiting chemical reactions between the substrate surface and alternating exposure to a precursor and co-reactant.[11]

Recently, mobilities of 0.5 $cm^2V^{-1}s^{-1}$, 1 $cm^2V^{-1}s^{-1}$ and 6 $cm^2V^{-1}s^{-1}$ and on-current/off-current (I_{On}/I_{Off}) ratios of 10^4, 10^6, and 10^2 have been reported for SnO deposited by temporal ALD, using bis(1-dimethylamino-2-methyl-2-butoxy)tin, $Sn(dmamb)_2$, bis(1-dimethylamino-2-methyl-2-propoxy)tin $Sn(dmamp)_2$ and N,N′-tert-Butyl-1,1-dimethylethylenediamine stannylene(II),[12–14] respectively, as the Sn precursor with an H_2O co-reactant. Whilst these results are promising for the development of p-type transistors by ALD, the low deposition rate of temporal ALD, coupled with the low reactivity of current precursor technology may ultimately hinder large area industrial applications. The development of high deposition rate processes (*i.e.* high growth per cycle and/or short cycle time) with atomic-level control, suitable for large-area applications, are therefore of paramount importance. High-throughput ALD can be obtained by improving two major aspects of the process; (i) upgrades in deposition hardware (*i.e.* deposition equipment and methodology), which have the potential to reduce the overall cycle time, and or (ii) improvement of the underpinning chemistries involved (*i.e.* the development of novel and chemically optimized precursors) which can increase the growth per cycle (GPC), and shorten overall cycle time, thus increasing deposition rate by harnessing higher reactivity with the substrate surface and co-reactant.

In conventional temporal ALD substrates are exposed to alternate precursor and co-reactant doses which are separated in time by extensive purge steps to eliminate precursor mixing and afford self-limited deposition in a cyclic fashion. In contrast to temporal ALD, spatial ALD (sALD) relies on spatial separation of precursor and co-reactant, *i.e.* the substrate moves underneath injector heads from which either precursor or co-reactant are continuously flowing. The reactants are spatially separated by inert gas curtains to prevent mixing and CVD-like reactions.[15] Such a technique can therefore afford cyclic and self-limiting deposition as in temporal ALD at a much higher deposition rate.[16,17] This makes sALD well-suited for highly

precise, high throughput, and in-line material processing over large areas, *e.g.* roll-to-roll and sheet-to-sheet sALD.[18–20]

ALD relies extensively on the underpinning reactive chemistry of precursors. As such the development of new and more reactive precursors is an essential method of improving GPC and overall deposition rate. Precursor design is well-known to have considerable impact on both rates of thin film growth as well as thin film properties.[21] In general, conventional wisdom on precursor design dictates that precursors must be sufficiently volatile and thermally stable, with high reactivity towards the substrate and surface film as well as the desired co-reagent (*i.e.* H_2O) to allow for self-limiting surface reactions. In the case of metastable materials such as SnO, an additional layer of sophistication is required within the precursor design, with the need for oxidative control, in order to ensure the phase purity of the as-deposited SnO, such that higher oxidation state materials (*i.e.* SnO_2) are not co-deposited. Lack of oxidative control has the potential to result in undesirable properties for p-type SnO TFT such as the evolution of n-type conductivity culminating in the inability to turn off the transistors. To this end, care must be taken to ensure that Sn present in the precursor is in the same oxidation state as that required in the desired thin film, necessitating the use of precursor molecules that display suitably high reactivity towards mild, non-oxidizing co-reagents such as H_2O.

Herein we report for the first time the sALD of phase pure SnO with improved deposition rate compared to conventional temporal ALD, through a synergistic combination of the development of an innovative and highly reactive Sn(II) alkoxide ALD precursor, tin(II)-bis(tert-amyloxide), $Sn(TAA)_2$,[22] and sALD technology, targeting improvements in both GPC and overall deposition cycle time. SnO films were grown at much improved deposition rates in comparison to temporal ALD, and p-type TFT behavior was demonstrated for proof-of-concept TFT devices fabricated using the deposition chemistry and processing described herein. The deployment of a novel ALD Sn(II) precursor in conjunction with a sALD process opens new

industrially relevant pathways for high-throughput and reliable p-type TFTs to be implemented in oxide semiconductor CMOS logic on large area and flexible substrates.

2. Results and Discussion

2.1. Precursor Development

In order to target volatile monomeric Sn(II) compounds, focus has typically been directed towards ligands capable of limiting molecular oligomerization either sterically or coordinatively, *i.e.* by incorporating lariat arms.[23] However, this approach also inherently renders the Sn(II) center less labile through a combination of steric and kinetic effects, reducing reactivity within an ALD process, which is compounded by the necessary use of mild co-reagents such as H_2O to maintain oxidative control of the Sn(II) film.

To date, very few molecular precursors, the lariat aminoalkoxide derivatives bis(1-dimethylamino-2-methyl-2-propoxy)tin, ($Sn(dmamp)_2$), and bis(1-dimethylamino-2-methyl-2-butoxy)tin, $Sn(dmamb)_2$, in addition to N,N′-tert-Butyl-1,1-dimethylethylenediamine stannylene(II) have been reported as being capable of forming crystalline and electronically suitable p-type tin(II) oxide via ALD,[12–14,24] with all processes displaying low growth rates when used in combination with H_2O, limiting the industrial applicability of these processes. Further to this, a number of studies report the deposition of mixed phase and amorphous SnO_x films and a short overview of SnO ALD processes with related deposition parameters and resulting TFT properties is provided in **Table 1**, for completeness a short overview of SnO processes other than ALD and the resulting TFT properties is also provided in **Table 2**. More comprehensive overviews, including device structures and dielectric layers, were published by Wang *et al.* and R. Barros *et al.*[5,25] The wide variability in the effectiveness of Sn-based precursors in terms of not only deposition rate, growth per cycle and deposition parameters, but as importantly features such as film composition, oxidative control, density, electrical

characteristics, purity and crystallinity emphasize the subtlety and impact of precursor design and the importance of iterative improvement within the field.

Whilst Sn(II) alkoxide systems, which do not contain ancillary lariat groups such as $\{NMe_2\}$, have not previously been considered ideal candidates as molecular precursors in deposition processes because of a perceived tendency to oligomerize and thus display low volatility, $Sn(TAA)_2$, upon distillation in vacuum, is a colorless liquid at room temperature with sufficient volatility and, based on similar chemical shift in ^{119}Sn nuclear magnetic resonance, a dimeric structure analogous to Sn(II)tert-butoxy, $Sn(O^tBu)_2$.[26] Unlike the monomeric, four-coordinate Sn(II) center in the aminoalkoxide $Sn(dmamp)_2$, the Sn centers in simple, dimeric alkoxides such as $Sn(TAA)_2$ and $Sn(O^tBu)_2$ adopt a three-coordinate configuration, with higher kinetic and thermodynamic lability than related chelating systems.[26]

Thermal stability and volatility of $Sn(TAA)_2$ were assessed via thermogravimetric analysis, which displayed a sharp mass loss consistent with volatility beginning at ca. 150 °C, affording a mass of 10% at 220 °C and a mass of 3% at 250 °C, well below that expected for thermal decomposition products Sn, SnO and SnO_2, as shown in **Figure 1**, and rendering $Sn(TAA)_2$, initially explored in the context of chemical vapor deposition,[26] a suitable candidate for ALD of SnO (see also Supporting Information, **Figure S1**). A small degree of stepped mass loss at higher temperatures (10%-3%) is not unexpected for metal alkoxide complexes, where in larger samples for which the ramp rate gradually exceeds the rate of evaporation, signs of decomposition become evident, as compounds reach their thermal tolerance. This assessment is an important aspect of precursor screening for ALD applications, where it must be ensured that the temperatures at which the process will operate remain below the thermal decomposition point of the precursor to be utilized.

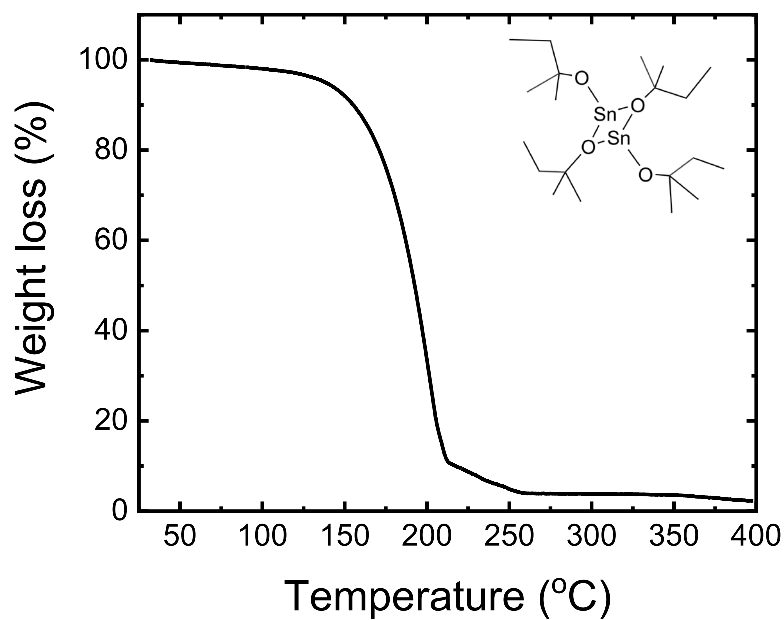

Figure 1. a) Thermogravimetric plot of Sn(TAA)$_2$. Analysis undertaken at a ramp rate of 5 °C min^{-1} with an Ar purge gas (20 mL min^{-1}). Inset: proposed dimeric structure of Sn(TAA)$_2$.

Table 1. Overview of ALD precursors for SnO_x, together with the deposition temperature, growth per cycle, annealing temperature and resulting TFT performance. In all cases the co-reactant is H_2O. (a) indicates the spatial ALD process as opposed to temporal ALD, (b) linear mobility as opposed to saturation mobility, and (c) the growth per cycles that were derived from Figures in the respective references. $Sn(edpa)_2$ = bis(N-ethoxy-2,2-dimethyl propanamido)tin. RTA = rapid thermal annealing, n.a. = not available.

Precursor	**Deposition temperature (°C)**	**Growth per cycle (Å)**	**Annealing temperature (°C)**	**Mobility $cm^2V^{-1}s^{-1}$**	**I_{On}/I_{Off}**	**Reference**
$Sn(TAA)_2^a$	100-210	0.55 - 0.09	250 in N_2 1 hr	0.4^b	6 x 10^2	*This work*
$Sn(dmamp)_2$	90-210	0.61-0.08	250 in N_2 1 hr	~1	2 x 10^6	[13]
$Sn(dmamp)_2$	200	0.1^c	1000 RTA in O_2	1.6	1.2 x 10^5	[27]
$Sn(dmamb)_2$	100-200	0.20-0.13	450 RTA in N_2	0.5	7 x 10^4	[12]
$Sn(edpa)_2$	70-300	0.26	n.a	n.a	n.a	[28]
bis[bis(trimethylsilyl) amino]tin(II)	100-250	00.18-0.05	n.a	n.a	n.a	[29]
N,N’ -tert-butyl-1,1-dimethylethylenediamine stannylene (II)	60-200	$00.5\text{-}0.1^c$	n.a	n.a	n.a	[30]
N,N′-tert-Butyl-1,1-dimethylethylenediamine stannylene(II)	100	0.1^c	300 in N_2 1 hr	6	2.7 x 10^2	[14]

Table 2. Overview of SnO_x deposition technologies together with the deposition temperature, annealing temperature and resulting TFT performance. DCMS = direct current magnetron sputtering; RFMS = radio frequency magnetron sputtering; PLD = pulsed laser deposition.

Deposition method	Deposition temperature (°C)	Annealing temperature (°C)	Mobility ($cm^2V^{-1}s^{-1}$)	I_{On}/I_{Off}	Reference
DCMS	RT	180 in air 30 min	6.75	~1.0 x 10^3	[31]
DCMS	RT	300 in O_2 30 min	6.54	1.0 x 10^5	[32]
PLD	300	300 1hr	2.18	5.4	[33]
PLD	RT	300 in O_2 30 min	1.47	~10^4	[34]
PLD	575	-	1.3	1.0 x 10^2	[35]
PLD	RT	250 in air 30 min	0.55	~1.0 x 10^2	[36]
PLD	500	n.a.	0.34	2.7 x 10^2	[37]
RFMS	90	n.a.	4.86	3.0 x 10^4	[38]
RFMS	RT	200 2hrs	1.36	1.5 x 10^3	[39]
RFMS	RT	200 100 s	1.2	2.5 x 10^4	[40]
RFMS	RT	225 in air 30 min	0.33	1.0 x 10^3	[41]
Spin coating	RT	450	0.13	85	[42]
Thermal evaporation	250	-	1.4	5.0 x 10^4	[43]

2.2 Spatial ALD of SnO.

Deposition studies were undertaken on a custom-built lab-scale sALD rotary reactor, a detailed description of which can be found in previous reports.[19] Within this set up, the substrate is rotated under gas streams of precursor and co-reagent, separated with an inert gas purge curtain, affording facile modification of precursor exposure time through variation of rotation speed. Initial depositions were carried out at substrate temperatures of 100 °C, 160 °C and 180 °C, with saturating behavior consistent with ALD, and indicative of self-limiting surface reactions and thermal stability of the precursor, observed for exposure times between 220 ms and 480 ms. GPC as a function of precursor and co-reactant exposure time is illustrated in **Figure 2**. $Sn(TAA)_2$ exposure times of 200 ms were required to achieve surface saturation, with shorter exposure times resulting in an unsaturated growth regime, as shown for the deposition temperature of 100 °C (Figure 2). GPC values of 0.55 Å, 0.36 Å and 0.19 Å were measured by spectroscopic ellipsometry (SE) for deposition temperatures of 100 °C, 160 °C and 180 °C, respectively.

A significant benefit offered by sALD is the reduction in overall cycle time and lengthy purge times when compared to temporal ALD, thereby increasing the rate of deposition. By establishing an optimized saturation time for both precursor and co-reagent, cycle times for deposition processes can be calculated by incorporating the times of each purge enacted by movement of substrate through the inert gas curtain. For the conditions used in these experiments the shortest exposure time for precursor and co-reactant to achieve saturating behavior was found to be 220 ms. Because of the fixed dimensions of the injector head, the shortest purge times were found to be 1.02 s for the precursor and 4.02 s for the H_2O co-reactant (see Experimental section for details). The shortest cycle time was calculated to be 5.42 s, though it is expected that purge duration can be decreased with further optimization. As an example, purge times down to few milliseconds have been demonstrated on the same setup for Al_2O_3 sALD on planar substrates.[15]

In order to provide a valuable comparison between the novel ALD precursor $Sn(TAA)_2$ and the previously reported thermal ALD precursor $Sn(dmamp)_2$, sALD process development was undertaken on both precursor systems. **Figure 3** depicts the saturation curves obtained for the sALD of SnO using $Sn(TAA)_2$ and $Sn(dmamp)_2$ as the Sn precursor at a deposition temperature of 160 °C. In the case of $Sn(TAA)_2$ exposure times of 220 ms were found to be sufficient for achieving saturating behavior, whilst more than 500 ms were found to be necessary for $Sn(dmamp)_2$. In addition to a shorter precursor dosing time and cycle time, a higher GPC was obtained for SnO deposited by $Sn(TAA)_2$. **Table 3** reports the deposition rate obtained for sALD using $Sn(TAA)_2$ and $Sn(dmamp)_2$ as the Sn precursors and provides comparison with those reported for temporal ALD using $Sn(dmamp)_2$ and $Sn(dmamb)_2$.[12,24,27] Depending on the deposition temperature, the sALD deposition rate using $Sn(TAA)_2$ was found to be between 2.6 and 1.5 times higher than that obtained using $Sn(dmamp)_2$ in the same sALD reactor. The deposition rates obtained with $Sn(TAA)_2$ sALD are also between 6 to 19.5, and 6 to 15 times higher when compared to those reported for temporal ALD using $Sn(dmamp)_2$ and $Sn(dmamb)_2$, respectively. Overall, it can be concluded that the shorter ALD cycle time obtainable using sALD is not only due to hardware (sALD vs temporal ALD) but also to the physico-chemical (vapor pressure and/or reactivity) properties of the $Sn(TAA)_2$ precursor itself.

In order to study the effect of the deposition temperature on GPC, and film properties, SnO layers of ca. 20 nm thickness were deposited at different substrate temperatures ranging from 100 °C to 210 °C. The substrate speed was set to 10 RPM, corresponding to exposure times ranging from 220 ms to 480 ms (*i.e.* within saturation regime) and purge times between 1.02 s to 1.28 s and 4.28 s to 4.02 s after $Sn(TAA)_2$ and H_2O respectively. As shown in **Figure 4**, the GPC decreases with increasing deposition temperature, decreasing from 0.55 Å at 100 °C to 0.09 Å at 210 °C. Similar behavior was observed in the case of SnO deposited by temporal ALD using $Sn(dmamp)_2$ and H_2O, a feature attributed to increased surface de-hydroxylation with increasing deposition temperature.[24]

The refractive index was measured by optical modelling of variable-angle spectroscopic ellipsometry (VASE) measurements, with the temperature-dependent refractive index, *n*, shown in **Figure 4**. Whilst the GPC decreases with increasing deposition temperature, *n* follows opposite trend, suggesting densification and crystallization of the SnO layers at higher deposition temperatures. Liang *et al.* have previously reported that the optical constants of SnO films are significantly influenced by the crystallinity of the layers.[44] At a deposition temperature of 100 °C a refractive index of 2.48 at photon energies of 1.96 eV was observed for films deposited at 100 °C, consistent with amorphous SnO.[44,45]

Table 3. Experimental deposition rates of SnO ALD: sALD using $Sn(TAA)_2$ and $Sn(dmamp)_2$; and temporal ALD using $Sn(dmamp)_2$ and $Sn(dmamb)_2$ as a function of deposition temperature. The ALD cycle time for sALD was 6 s using $Sn(TAA)_2$ and 10 s using $Sn(dmamp)_2$, whilst cycle times reported for temporal ALD using $Sn(dmamp)_2$ are 31 s, [13] 36.5 s,[27] and 31 s using $Sn(dmamb)_2$.[12] a) These data were obtained using the same sALD tool described in this work.

Deposition temperature (°C)	SnO deposition rate (nm/min)				
	Spatial ALD		Temporal ALD		
	$Sn(TAA)_2$	**$Sn(dmamp)_2$[a]**	**$Sn(dmamp)_2$[13]**	**$Sn(dmamp)_2$[27]**	**$Sn(dmamb)_2$[12]**
100	0.60	0.23	0.09	0.07	0.04
160	0.39	0.17	0.03	0.02	0.03
190	0.18	0.12	0.02	0.02	0.03

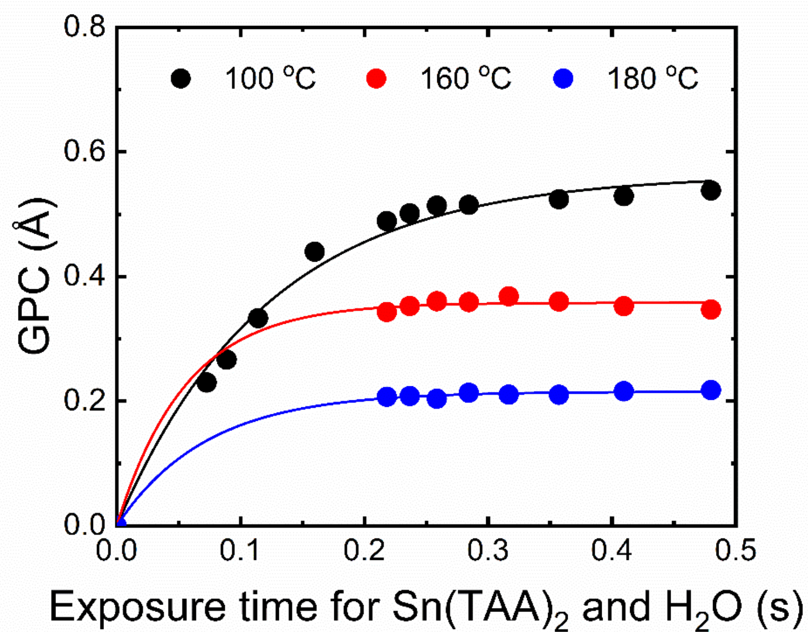

Figure 2. Growth per cycle as a function of the exposure time for deposition temperatures of 100 °C, 160 °C and 180 °C. The data points were fitted using a Langmuir adsorption model.

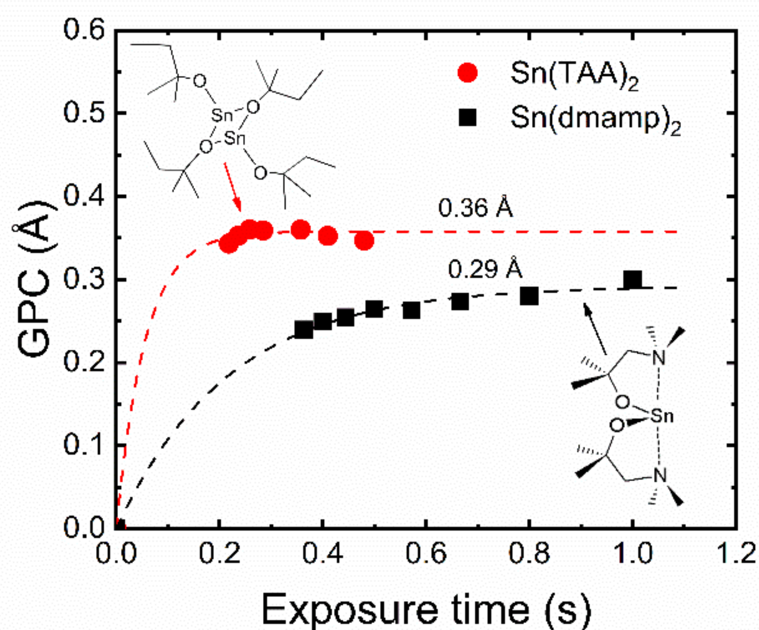

Figure 3. SnO growth per cycle as function of the overall exposure time using $Sn(TAA)_2$ (red circles) and $Sn(dmamp)_2$ (black squares).

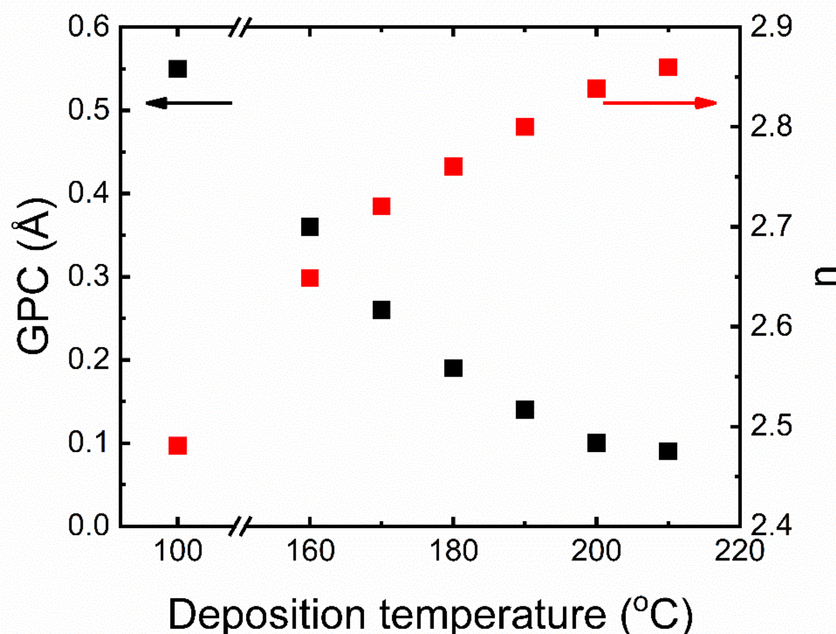

Figure 4. Growth per cycle as measured by ex-situ variable angle spectroscopic ellipsometry (VASE) as a function of deposition temperature. The SnO refractive index is reported at a wavelength of 1.96 eV. All SnO layers were ca. 20 nm thick.

The refractive index of the as deposited films increases to 2.65 at a deposition temperature of 160 °C, 2.72 at 170 °C, and 2.86 at 210 °C. Concurrently, the optical energy gap, E_{gap}, estimated by linear fitting of $\alpha h\nu^{1/2}$ as function of the photon energy, $h\nu$, increases from 2.29 eV at 100 °C to 2.45 at 170 °C (see Supporting Information **Figure S2** for details). These results point at a SnO crystallization temperature of ca. 170 °C for the described process.

Bragg-Brentano, θ-2θ, X-ray diffraction studies of 10 nm films deposited at 190 °C confirm the presence of crystalline SnO (**Figure 5a**). The reflections at 2θ values of 18.3 and 37.0 degrees were attributed to the (001) and (002) planes of SnO, indicating a highly oriented film. Such preferred orientation is consistent with film growth in the plane of the a and b axes, parallel with the substrate surface, as would be expected for SnO growth in an Sn-O-Sn fashion, and is consistent with that observed in the layered, tetragonal litharge SnO unit cell.[46] As shown in **Figure 5b**, Raman spectroscopy also reveals signals at 109 cm^{-1} and 211 cm^{-1},

attributed to the characteristic E_g and A_{1g} vibrational modes of SnO respectively,[47,48] in addition to a substrate peak at 309 cm^{-1} (Si 2TA).

XPS was used to confirm the presence of SnO through modelling of the Sn(II):Sn(IV) ratio. Variability within reported XPS data for SnO and SnO_2 requires a cautious approach, where possible confirming a correct assessment through corroboration of a range of data including the modelling of $Sn3d_{5/2}$ peak contributions (**Figure 5c**), the relative position of the 3d peaks with respect to the O1s peak as well as assessment of the Sn valence band region if obtainable. In the case of films deposited in this study, XPS indicates a Sn(II) content of 89 % (Sn(II) $3d_{5/2}$ = 486.10 eV), with minority contributions from Sn(IV) (4 %, $3d_{5/2}$ = 486.60 eV) and Sn(0) (7 %, $3d_{5/2}$ = 484.56 eV). This composition confirms the presence of bulk SnO with only minor contributions of SnO_2 and Sn. This result is also corroborated by Raman and XRD analysis and is consistent with literature precedent.[24,49] Full analytical detail is provided in the Supporting Information.

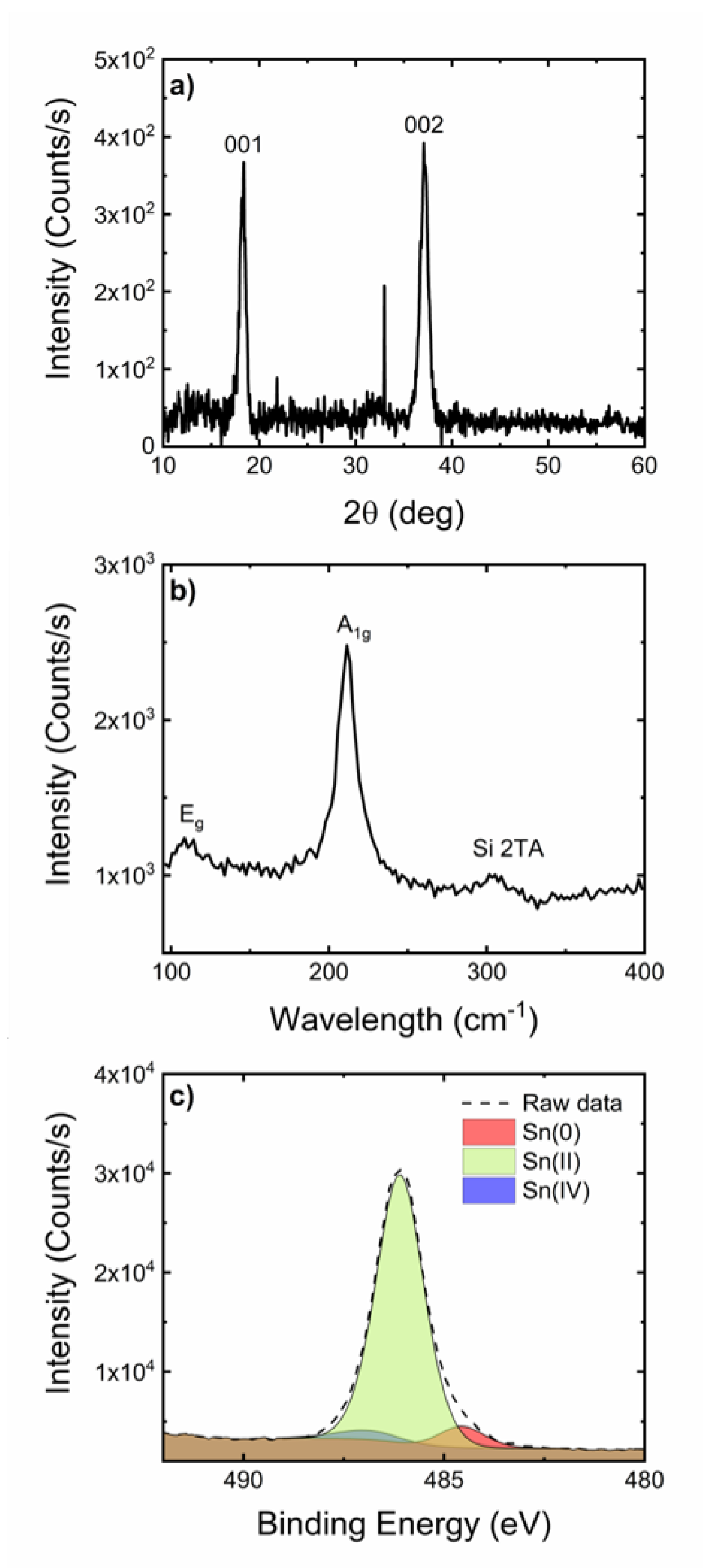

Figure 5. a) θ-2θ XRD scan, **b)** Raman spectrum, and **c)** core level XPS scan of the $Sn3d_{5/2}$ peak for a 10 nm thick SnO film deposited at 190 °C. 109 cm^{-1} (E_g) and 211 cm^{-1} (A_{1g}) 309 cm^{-1} (Silicon 2TA).

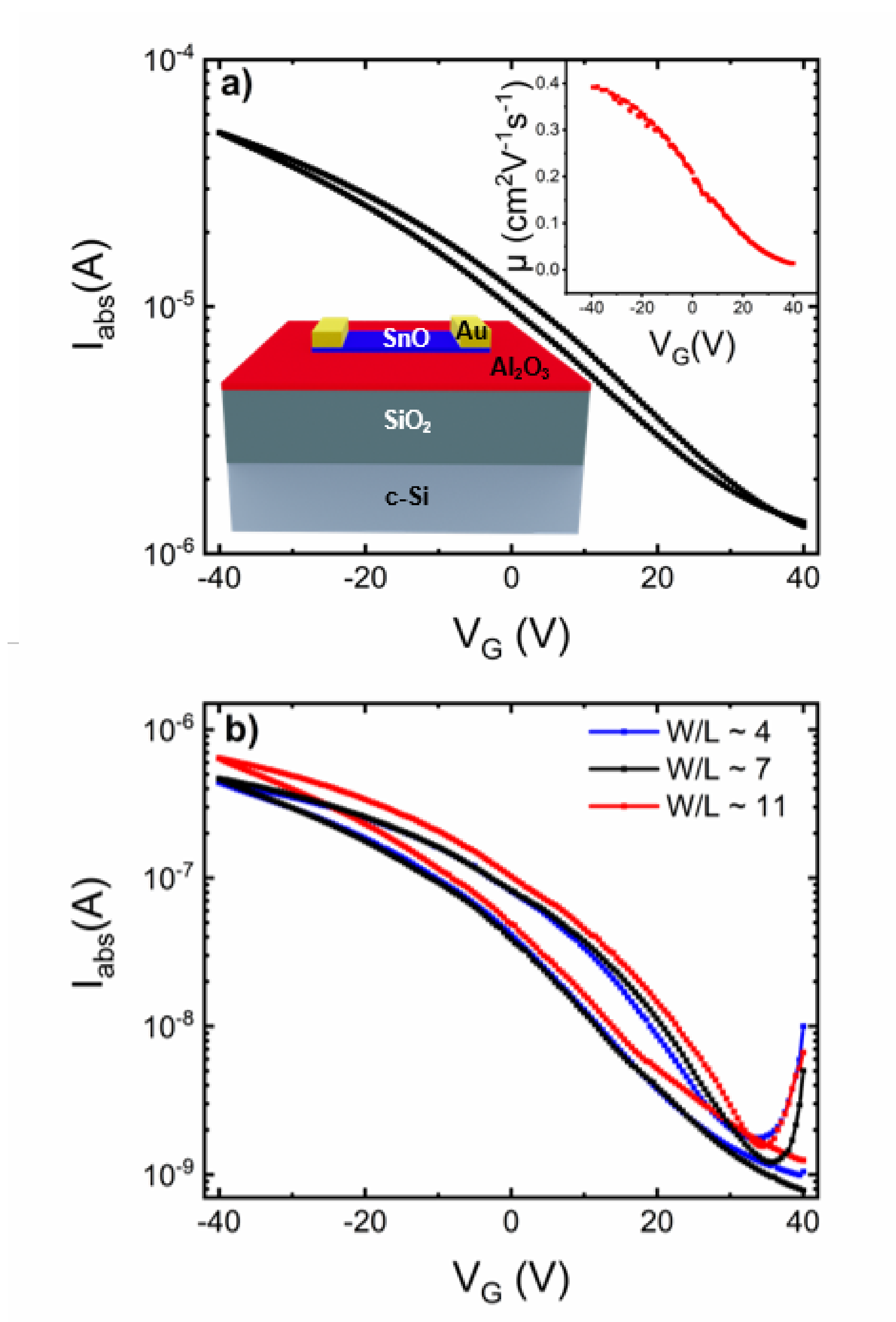

Figure 6. Transfer characteristics for SnO common-gate TFTs deposited by sALD at a deposition temperature of **a)** 200 ºC and **b)** 190 ºC. The inset of Figure 6a shows the extracted linear mobility. All TFTs were not encapsulated.

2.2. TFT results.

Crystallinity of SnO has been reported to be necessary to achieve high hole mobility and preferential orientation is purported to play a major role in terms of device performance.[13,50,51] Proof-of-concept TFTs were fabricated with SnO deposited at temperatures between 170 and 200 °C in accordance with the expected crystallinity within this temperature window. p-type behavior was observed for all investigated deposition temperatures. Upon annealing the TFTs for 1 hr in N_2 at 250 °C, the highest I_{On} was obtained for the SnO deposited at 200 °C, which led to linear field effect mobilities up to 0.4 $cm^2V^{-1}s^{-1}$ as shown in **Figure 6a**. The highest I_{On}/I_{Off}, however, was obtained at a deposition temperature of 190 °C, reaching values between 4 x 10^2 and 6 x 10^2, see **Figure 6b**. Additional transfer characteristics are reported in the Supporting Information, **Figure S4** and **Figure S5**. For comparison, similar TFT structures realized using sALD and $Sn(dmamp)_2$ as the Sn(II) precursor resulted in mobilities comparable to previously reported values using the same precursor, but lower I_{On}/I_{Off}, *i.e.* $1 \cdot 10^2$.[13] The sALD process using $Sn(dmamp)_2$ underwent no further exploration due to the higher efficiency of the $Sn(TAA)_2$ sALD process, which demonstrated greater promise for industrial application, where compromises between performance and throughput are emphasized. It should be noted that in both cases a reasonably positive on-voltage, V_{On}, was obtained, indicating a relatively highly-doped semiconductor, resulting in high current at V_G = 0 V. This behavior might be attributed to the lack of encapsulation layers and unoptimized annealing step which is the subject of ongoing investigations.

3. Conclusion

In attempts to rationalize a high deposition rate process for SnO through concerted improvements in both methodology and the underpinning chemistry, we have demonstrated for the first time a scalable deposition process with atomic-level control over thickness and material properties using atmospheric pressure sALD and a novel tin(II) ALD precursor, tin(II) bis-tert-

amyl alkoxide, $Sn(TAA)_2$. The self-limiting behavior of the sALD process for SnO has been validated over a wide temperature range (100-180 °C) demonstrating excellent thermal stability and suitability of $Sn(TAA)_2$ within ALD processes. The GPC of the p-type SnO film was found to decrease from 0.55 Å to 0.09 Å with increasing deposition temperature from 100 °C to 210 °C.

Through application of a reactive precursor and in conjunction with sALD processing, extraordinary growth rates, up to 19.5 times faster, were achieved compared to temporal ALD of SnO providing the fastest growth rates of crystalline p-type SnO to date. Developments such as this are essential in paving the way for high-throughput sALD of p-type semiconducting metal oxides on large area and flexible substrates with atomic-level precision. Translation of the previously reported temporal ALD precursor $Sn(dmamp)_2$ to a spatial ALD process allowed for comparison of reactivity, saturation and growth rates with the precursor catalogued within this study, $Sn(TAA)_2$, demonstrating the improved deposition behavior of SnO using $Sn(TAA)_2$. Crystalline SnO was deposited at temperatures over 170 °C, with as deposited films characterized by spectroscopic ellipsometry, XRD, Raman and XPS studies.

SnO films deposited by sALD exhibited p-type behavior as demonstrated by common-gate TFTs. The highest mobility obtained in proof-of-concept common-gate devices was 0.4 $cm^2V^{-1}s^{-1}$ for 19 nm thick SnO layers deposited at 200 °C, while an on-current/off-current ratio up to $6 \cdot 10^2$ was obtained for SnO deposited at 190 °C. The ALD of SnO using $Sn(TAA)_2$ alongside the exploration of doping and encapsulation strategies to maximize the performance of the resulting p-type devices will be investigated in the near future. The results presented in this work highlight the importance of concerted improvements in both precursor chemistry and deposition technology for advancing industrially-compatible atomic-level processing and engineering of p-type materials on large area substrates.

4. Experimental Section

Precursor synthesis: $Sn(TAA)_2$ was synthesized as previously reported under standard Schlenk conditions via the addition of 2-methyl-2-butanol to a cooled solution of Sn(II) bis-trimethylsilyl amide, $Sn(HMDS)_2$, in hexane.[26] A colorless liquid, $Sn(TAA)_2$, was isolated and purified by vacuum distillation after removal of the volatiles in vacuo.

Deposition studies: An atmospheric pressure dielectric barrier discharge (DBD) plasma source operated at a voltage of 125 V and frequency of 66 kHz was employed for depositing the Al_2O_3 buffer layer for the TFTs samples. Trimethylaluminum (TMA) was used as the precursor with an Ar bubbling flow of 75 sccm and additional 925 sccm of Ar as dilution. For the plasma co-reactant, 100 sccm of O_2 diluted in 9900 sccm of N_2 were used as plasma feeding gas. All Al_2O_3 buffer layers were deposited at 160 °C for 540 sALD cycles at a rotation frequency of 60 RPM, resulting in a 45 nm thick layer.

For the SnO deposition, the $Sn(TAA)_2$ bubbler was heated to 70 °C in order to ensure sufficient vapor pressure, 700 sccm of Ar were bubbled through the liquid precursor and 300 sccm of Ar were added as downstream dilution. Rotation speeds were decreased from 30 RPM to 10 RPM to derive the saturation curve of the process at 100 °C. All TFT depositions were carried out at 10 RPM to ensure deposition uniformity.

Because of the reactor construction, the exposure time of the substrate to the precursors/co-reactant, t_{exp}, is calculated using Equation 1:

$$t_{exp} = \frac{L}{2\pi r\ RPM} \tag{1}$$

where L is the width of the deposition zone (1.2 cm), r the radial distance from the center of the wafer, and RPM the rotations per minute.

Analytical methods: The growth of SnO was investigated by depositing on 150 mm Si (100) wafers. SnO thickness and optical properties were measured by ex-situ variable angle spectroscopic ellipsometry (VASE), using a Horiba UVISEL II, in the range from 1.5 eV to 5.5

eV. The angle of incidence was varied from 60° to 80° in steps of 10°. A single or a double Tauc-Lorentz model was used to fit the optical response of the SnO layers, as described by Liang *et al.*[44] Thermogravimetric analysis was carried out on a Perkin Elmer TGA 4000 in an argon-filled glovebox. Raman spectroscopy was undertaken on a Renishaw inVia using a 532 nm laser. Bragg-Brentano θ-2θ X-ray diffraction (XRD) was carried out on a STOE Stadi P reflection diffractometer. X-ray photoelectron spectroscopy (XPS) was undertaken using an Thermo Escalab 250 UHV-XPS system.

TFT fabrication and characterization: Common gate TFTs were fabricated on 150 mm highly doped c-Si (100) with 300 nm thermally grown SiO_2 and additional 45 nm Al_2O_3 sALD-grown buffer layer atop. SnO layers were deposited using sALD. The layers were patterned using photolithography and wet etching (5% oxalic acid solution in H_2O). After patterning, source-drain contacts were created by evaporating Au through a shadow mask with varying lengths (L) and fixed width (W) of 2000 µm. Annealing was performed after Au patterning for 1 hr in an N_2 environment at a temperature of 250 °C. The back contact was created by scratching the SiO_2 at the backside of the wafer and contacted with Ag paste. All TFTs were measured under N_2 atmosphere using an Agilent 4155C semiconductor parameter analyzer connected to a semiautomatic prober.

Supporting Information

Supporting Information is available from the Wiley Online Library or from the author.

Acknowledgements

The authors are thankful to Ilias Katsouras for fruitful discussions. Leslye Ugalde and Thijs Bel are greatly acknowledged for their technical support. The authors would also like to thank Andrew Brookes, the Chemical Characterization and Analysis Facility, University of Bath, and

Dr Andrew Britton of the Henry Royce Institute, University of Leeds, for their assistance and input on characterization. This work was partially financed by the King Abdullah University of Science and Technology (KAUST) Office for Sponsored Research (OSR) under Award OSR-CRG2018-3783. We also gratefully acknowledge the EPSRC and University of Bath for a departmental funded studentship (JDP), and the University of Bath Department of Chemistry for their support of MWS.

Received: ((will be filled in by the editorial staff))
Revised: ((will be filled in by the editorial staff))
Published online: ((will be filled in by the editorial staff))

References

[1] E. Fortunato, P. Barquinha, R. Martins, *Adv. Mater.* **2012**, *24*, 2945.

[2] D. H. Kim, M. D. Losego, Q. Peng, G. N. Parsons, *Adv. Mater. Interfaces* **2016**, *3*, 1.

[3] G. Gregory, C. Luderer, H. Ali, T. S. Sakthivel, T. Jurca, M. Bivour, S. Seal, K. O. Davis, *Adv. Mater. Interfaces* **2020**, *7*, 1.

[4] W. P. Zhang, S. B. Qian, W. J. Liu, S. J. Ding, D. W. Zhang, *IEEE Electron Device Lett.* **2015**, *36*, 1021.

[5] Z. Wang, P. K. Nayak, J. A. Caraveo-Frescas, H. N. Alshareef, *Adv. Mater.* **2016**, *28*, 3831.

[6] Z. W. Shang, H. H. Hsu, Z. W. Zheng, C. H. Cheng, *Nanotechnol. Rev.* **2019**, *8*, 422.

[7] M. Rockele, K. Vasseur, A. Mityashin, R. Muller, A. Chasin, M. Nag, A. Bhoolokam, J. Genoe, P. Heremans, K. Myny, *IEEE Trans. Electron Devices* **2018**, *65*, 514.

[8] J. Zhang, J. Yang, Y. Li, J. Wilson, X. Ma, Q. Xin, A. Song, *Materials (Basel).* **2017**, *10*, 1.

[9] A. Mameli, M. J. M. Merkx, B. Karasulu, F. Roozeboom, W. (Erwin) M. M. Kessels, A. J. M. Mackus, *ACS Nano* **2017**, *11*, 9303.

[10] S. M. George, *Chem. Rev.* **2010**, *110*, 111.

[11] M. Leskelä, M. Ritala, *Angew. Chemie - Int. Ed.* **2003**, *42*, 5548.

[12] M. G. Chae, S. H. Han, B. K. Park, T. M. Chung, J. H. Han, *Appl. Surf. Sci.* **2021**, *547*, 148758.

[13] S. H. Kim, I. H. Baek, D. H. Kim, J. J. Pyeon, T. M. Chung, S. H. Baek, J. S. Kim, J. H. Han, S. K. Kim, *J. Mater. Chem. C* **2017**, *5*, 3139.

[14] H. M. Kim, S. H. Choi, H. J. Jeong, J. H. Lee, J. Kim, J. S. Park, *ACS Appl. Mater. Interfaces* **2021**, *13*, 30818.

[15] P. Poodt, A. Lankhorst, F. Roozeboom, K. Spee, D. Maas, *Adv. Mater.* **2010**, *22*, 3564.

[16] D. Muñoz-Rojas, V. H. Nguyen, C. Masse de la Huerta, S. Aghazadehchors, C. Jiménez, D. Bellet, *Comptes Rendus Phys.* **2017**, *18*, 391.

[17] V. H. Nguyen, A. Sekkat, C. Jiménez, D. Muñoz, D. Bellet, D. Muñoz-Rojas, *Chem. Eng. J.* **2021**, *403*, 126234.

[18] M. A. Mione, I. Katsouras, Y. Creyghton, W. van Boekel, J. Maas, G. Gelinck, F. Roozeboom, A. Illiberi, *ECS J. Solid State Sci. Technol.* **2017**, *6*, N243.

[19] A. Illiberi, I. Katsouras, S. Gazibegovic, B. Cobb, E. Nekovic, W. van Boekel, C. Frijters, J. Maas, F. Roozeboom, Y. Creyghton, P. Poodt, G. Gelinck, *J. Vac. Sci. Technol. A Vacuum, Surfaces, Film.* **2018**, *36*, 04F401.

[20] I. Katsouras, C. Frijters, P. Poodt, G. Gelinck, A. J. Kronemeijer, *J. Soc. Inf. Disp.* **2019**, *27*, 304.

[21] A. L. Johnson, J. D. Parish, in *Organomet. Chem.* (Ed.: P.I.P. Patmore, N.J.; Elliott), RSC, **2019**, pp. 1–53.

[22] J. D. Parish, A. L. Johnson, *Atomic Layer Deposition Method of Metal (II), (0), or (IV) Containing Film Layer*, **2021**, WO 2021/058986 A1.

[23] R. Dasgupta, S. Khan, in *Adv. Organomet. Chem.* (Ed.: P. Perez), Elsevier Inc., **2020**, pp. 105–152.

[24] J. H. Han, Y. J. Chung, B. K. Park, S. K. Kim, H. S. Kim, C. G. Kim, T. M. Chung, *Chem. Mater.* **2014**, *26*, 6088.

[25] R. Barros, K. J. Saji, J. C. Waerenborgh, P. Barquinha, L. Pereira, E. Carlos, R. Martins, E. Fortunato, *Nanomaterials* **2019**, *9*, DOI 10.3390/nano9030320.

[26] M. S. Hill, A. L. Johnson, J. P. Lowe, K. C. Molloy, J. D. Parish, T. Wildsmith, A. L. Kingsley, *Dalt. Trans.* **2016**, *45*, 18252.

[27] Y. Jang, I. W. Yeu, J. S. Kim, J. H. Han, J. H. Choi, C. S. Hwang, *Adv. Electron. Mater.* **2019**, *5*, 1.

[28] H. Y. Kim, J. H. Nam, S. M. George, J. S. Park, B. K. Park, G. H. Kim, D. J. Jeon, T. M. Chung, J. H. Han, *Ceram. Int.* **2019**, *45*, 5124.

[29] J. Tupala, M. Kemell, M. Mattinen, K. Meinander, S. Seppälä, T. Hatanpää, J. Räisänen, M. Ritala, M. Leskelä, *J. Vac. Sci. Technol. A Vacuum, Surfaces, Film.* **2017**, *35*, 041506.

[30] J. H. Lee, M. Yoo, D. Kang, H. M. Lee, W. H. Choi, J. W. Park, Y. Yi, H. Y. Kim, J. S. Park, *ACS Appl. Mater. Interfaces* **2018**, *10*, 33335.

[31] J. A. Caraveo-Frescas, P. K. Nayak, H. A. Al-Jawhari, D. B. Granato, U. Schwingenschlögl, H. N. Alshareef, *ACS Nano* **2013**, *7*, 5160.

[32] C. W. Zhong, H. C. Lin, K. C. Liu, T. Y. Huang, *IEEE Electron Device Lett.* **2015**, *36*, 1053.

[33] P.-C. Hsu, C.-C. Wu, H. Hiramatsu, T. Kamiya, H. Hosono, *ECS J. Solid State Sci. Technol.* **2014**, *3*, Q3040.

[34] C. W. Zhong, H. Y. Tsai, H. C. Lin, K. C. Liu, T. Y. Huang, *Proc. Int. Symp. Phys. Fail. Anal. Integr. Circuits, IPFA* **2015**, *2015-August*, 84.

[35] Y. Ogo, H. Hiramatsu, K. Nomura, H. Yanagi, T. Kamiya, M. Hirano, H. Hosono, *Appl. Phys. Lett.* **2008**, *93*, 1.

[36] K. Nomura, T. Kamiya, H. Hosono, *Adv. Mater.* **2011**, *23*, 3431.

[37] M. Liao, Z. Xiao, F.-Y. Ran, H. Kumomi, T. Kamiya, H. Hosono, *ECS J. Solid State Sci. Technol.* **2015**, *4*, Q26.

[38] U. Myeonghun, Y. J. Han, S. H. Song, I. T. Cho, J. H. Lee, H. I. Kwon, *J. Semicond. Technol. Sci.* **2014**, *14*, 666.

[39] H. Luo, L. Y. Liang, Q. Liu, H. T. Cao, *ECS J. Solid State Sci. Technol.* **2014**, *3*, Q3091.

[40] Y. J. Han, Y. J. Choi, I. T. Cho, S. H. Jin, J. H. Lee, H. I. Kwon, *IEEE Electron Device Lett.* **2014**, *35*, 1260.

[41] I. C. Chiu, Y. S. Li, M. S. Tu, I. C. Cheng, *IEEE Electron Device Lett.* **2014**, *35*, 1263.

[42] K. Okamura, B. Nasr, R. A. Brand, H. Hahn, *J. Mater. Chem.* **2012**, *22*, 4607.

[43] M. P. Hung, J. Genoe, P. Heremans, S. Steudel, *Appl. Phys. Lett.* **2018**, *112*, 2635021.

[44] L. Y. Liang, Z. M. Liu, H. T. Cao, Y. Y. Shi, X. L. Sun, Z. Yu, A. H. Chen, H. Z. Zhang, Y. Q. Fang, *ACS Appl. Mater. Interfaces* **2010**, *2*, 1565.

[45] L. Y. Liang, Z. M. Liu, H. T. Cao, Z. Yu, Y. Y. Shi, A. H. Chen, H. Z. Zhang, Y. Q. Fang, X. L. Sun, *J. Electrochem. Soc.* **2010**, *157*, H598.

[46] K. J. Saji, K. Tian, M. Snure, A. Tiwari, *Adv. Electron. Mater.* **2016**, *2*, 1.

[47] Q. Liu, L. Liang, H. Cao, H. Luo, H. Zhang, J. Li, X. Li, F. Deng, *J. Mater. Chem. C* **2015**, *3*, 1077.

[48] J. Geurts, S. Rau, W. Richter, F. J. Schmitte, *Thin Solid Films* **1984**, *121*, 217.

[49] J. Heo, A. S. Hock, R. G. Gordon, *Chem. Mater.* **2010**, *22*, 4964.

[50] P. C. Hsu, W. C. Chen, Y. T. Tsai, Y. C. Kung, C. H. Chang, C. C. Wu, H. H. Hsieh, *Thin Solid Films* **2014**, *555*, 57.

[51] A. Togo, F. Oba, I. Tanaka, K. Tatsumi, *Phys. Rev. B - Condens. Matter Mater. Phys.* **2006**, *74*, 1.

Table of contents

High-rate Atomic Layer Deposition of p-type SnO. A novel precursor for SnO atomic layer deposition (ALD) is presented and employed for the first time in spatial ALD. The synergy between precursor chemistry and deposition hardware allows to achieve up to 19.5 times faster deposition with good p-type electrical performance. Linear mobilities up to 0.4 $cm^2V^{-1}s^{-1}$ are demonstrated with common gate thin film transistors.

A.M. Corresponding Author*, J.D.P. Author 2, T.D. Author 3, G.G. Author 4, M.W.S. Author 5 A.J.S. Author 6, A.L.J. Corresponding Author**, A.J.K. Author 8

*E-mail: alfredo.mameli@tno.nl
**E-mail: chsalj@bath.ac.uk

High-Throughput Atomic Layer Deposition of p-Type SnO Thin Film Transistors Using Tin(II)bis(tert-amyloxide)

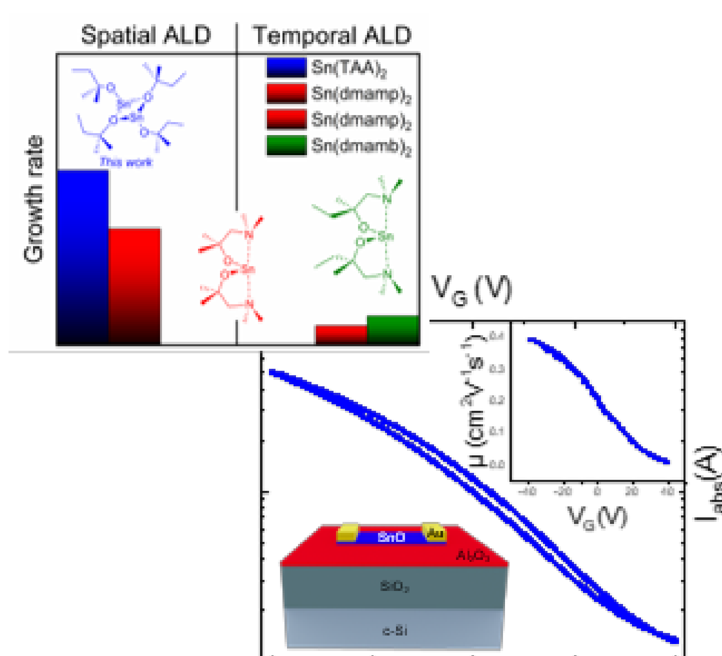

TOC 55 mm x 50 mm below: